Research Article | Vol. 30, No. 26 / 19 Dec 2022 / Optics Express 46307
Optics EXPRESS

Restraint of the mid-spatial frequency error on optical surfaces by multi-jet polishing

ZILI ZHANG,[1] CHI FAI CHEUNG,[1,*] CHUNJIN WANG,[1,3] LAI TING HO,[1] AND JIANG GUO[2]

[1] *State Key Laboratory of Ultra-precision Machining Technology, Department of Industrial and Systems Engineering, The Hong Kong Polytechnic University, Hung Hom, Kowloon, Hong Kong, China*
[2] *Key Laboratory for Precision and Non-traditional Machining of Ministry of Education, Dalian University of Technology, Dalian, China*
[3] *chunjin.wang@polyu.edu.hk*
[*] *Benny.Cheung@polyu.edu.hk*

Abstract: Nowadays, the mid-spatial frequency (MSF) error existing in the optical surface after polishing is still a great challenge for the ultra-precision manufacturing of optical components. MSF error severely deteriorates the performances of optical components such as causing small-angle scattering and reducing imaging contrast. In this paper, multi-jet polishing (MJP) was proposed to restrain the MSF error, whose tool influence function (TIF) was relatively more complicated and adjustable than the TIFs of other tools. The results demonstrated that MJP had a superior ability to reduce the ripple error, and the path spacing and nozzle orientation angle both had a significant effect on the MSF error of the polished surface. The optimization of nozzle orientation angle under different path spacings was conducted to achieve a high surface quality. This study contributes to the ultra-precision manufacturing of optical components, achieving a low MSF error together with high finishing efficiency.

1. Introduction

Computer-controlled polishing (CCP) technology has been used in the ultra-precision manufacturing of optical components by Jones *et al.* [1] for decades. In this process, high form accuracy was achieved by controlling the dwell time of the sub-aperture tool in different positions [2–4]. Among these manufacturing technologies, fluid jet polishing (FJP) has been extensively utilized in the surface finishing of optical components and molds due to its distinctive advantages such as the superior ability to polish the freeform surface, no tool wear, and high form accuracy [5,6]. Furthermore, multi-jet polishing (MJP) was proposed to enhance manufacturing efficiency as well [7–9]. However, a big challenge is that mid-spatial frequency (MSF) error occurs in this process, which is hard to be removed by later post-processing [10,11]. MSF error deteriorates the performances of optical components such as causing small-angle scattering and reducing imaging contrast [12–15]. As a result, it is of great importance to reduce the MSF error in CCP.

Wan *et al.* [16] investigated the MSF error characteristics and generation mechanism. It was found that different parameters including path type, tool influence function (TIF), feed rate, and movement type affected MSF error. To reduce MSF error, various solutions have been proposed. Most research focused on special tool path planning. The pseudo-random path was first proposed to reduce MSF error by Dunn, et al. [17]. Different types of non-periodic pseudo-random paths were further designed in the later studies such as unicursal random maze tool path [18], six-directional pseudorandom consecutive unicursal polishing path [19], circular-random path [20,21], hyper-crossing tool path based on the randomized epicyclical motion [22]. Zha proposed the pseudo-random path generation algorithms by changing the path direction and interval [23]. However, these tool paths were random and the motion had a high requirement for the acceleration and deceleration of the machine axes. Besides, the instability of the feed rate made

#473235 https://doi.org/10.1364/OE.473235
Journal © 2022 Received 15 Aug 2022; revised 31 Oct 2022; accepted 3 Nov 2022; published 6 Dec 2022

Optics EXPRESS

it hard to achieve a high form accuracy [17]. Some previous research work demonstrated that small path spacing was beneficial to the reduction of MSF error [10,24]. Nevertheless, for a certain material removal amount, the small path spacing leads to a high feed rate. Hence, the path spacing cannot be reduced infinitely due to the limitation of the machine tool. Hou *et al.* [25] applied a multi-pitch tool path to the CCP process, obtaining a lower MSF error together with higher form accuracy. Wang *et al.* [26] utilized a small pitch tool to reduce MSF error from 2.155 nm to 0.267 nm. Jing *et al.* [27] developed a semirigid bonnet tool to change the shape of TIF. The experiments indicated that the TIF with a Gaussian-like shape had the highest probability to generate lower MSF error than the trapezoidal shape and "W" shape TIFs. Due to the limitation of TIF shape, this method was complicated or not available to other manufacturing processes such as FJP with a "W" shape TIF. The sparse "bi-step raster path" was proposed to achieve efficient periodic ripple error removal by suppressing the first two-order peaks of the initial surface error spectrum [28]. Wang *et al.* [29] reduced the MSF error by heat treatment. However, this processing method was not effective enough to remove the ripple on the surface.

Despite the research efforts placed on the restraint of MSF error in optical component manufacturing, few of them can apply to FJP directly without any limitation. To enhance the polishing efficiency of FJP and meet the requirements of mass production, MJP was utilized and investigated, improving the manufacturing efficiency dozens of times [9]. The TIF of MJP can be easily adjusted by the arrangement of orifices on the nozzle. Besides, the material removal distribution of MJP is random, which is beneficial to the reduction of ripple error under a certain condition. Hence, there is the potential to achieve a low MSF error by MJP. However, the effect of MJP on the MSF error has not been elucidated.

In this paper, the reduction of the MSF error by MJP was proposed. MJP tool with seven orifices was designed and fabricated. The performance of MJP and single jet polishing (SJP) in restraining MSF error was investigated. Besides, the influence of different parameters including path spacing and nozzle orientation angle on MSF error was demonstrated. In addition, the optimization of the nozzle orientation angle was conducted to achieve a higher surface quality together with high polishing efficiency.

2. Methods

2.1. Principle of MJP

In traditional FJP, only one orifice is fabricated in the nozzle. The pressured water mixed with abrasives is released from the orifice and interact with the workpiece surface to achieve material removal. However, the material removal rate is low due to its small influence spot. As a result, MJP was proposed by fabricating more than one orifice in the nozzle and multiple jets interacted with the workpiece surface simultaneously to enhance the material removal rate. Figure 1 shows the principle of MJP. The design of the MJP tool, including the number and distribution of orifices, can be adjusted according to the requirements.

2.2. Theoretical method for restraining MSF error

To demonstrate the effectiveness of MJP in restraining the MSF error, a theoretical analysis was conducted based on surface generation characteristics in this section. First, the surface generation model was built to simulate the overlap of footprints and the cross-section profile of the generated surface in MJP and SJP. Based on the surface generation analysis, the reason for the restrained MSF error by MJP was revealed. The effect of nozzle angle on the MSF error was also elucidated, which laid down a theoretical foundation for the optimization of nozzle orientation angle to achieve the lowest MSF error in MJP.

Optics EXPRESS

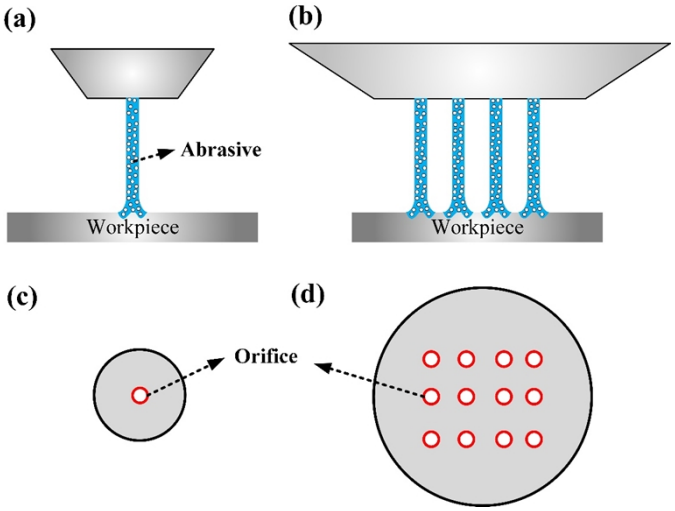

Fig. 1. The principle of MJP (a) the jet in SJP (b) the distribution of jets in MJP (c) the nozzle design of SJP (d) the nozzle design of MJP.

In FJP, the TIF is obtained by the experiment and considered as constant [30]. The generated surface after polishing can be expressed as

$$H(x, y) = TIF(x, y) * t(x, y) \tag{1}$$

where $H(x, y)$ is the generated surface; $TIF(x, y)$ is the TIF obtained by the experiment; $t(x, y)$ is the dwell time distribution during polishing.

Figure 2(a1) and Fig. 2(b1) show the TIFs of SJP and MJP. The cross-section profile of SJP's TIF had a regular 'M' shape, while the cross-section profile of MJP's TIF was random. The material removal difference was caused by the increasing number of orifices and the flow field interference among adjacent jets. The random material removal distribution is beneficial to the restraint of MSF error resulting from the periodic ripples. Besides, unlike the cylindrically symmetric 'M' shape TIF in SJP, the TIF of MJP was closely dependent on the nozzle orientation. Changing the nozzle orientation by rotating the nozzle can obtain a different material removal distribution on the workpiece. As a result, MJP can provide an additional approach for the restraint of MSF error.

The material removal process in FJP can be divided into two parts [31]. First, the material is removed along the feed rate direction. Second, the material removal along different path lines overlaps and the interval equals the corresponding path spacings. According to Eq. (1), Fig. 2(a2), Fig. 2(b2), and Fig. 2(c2) show the material removal and the corresponding cross-section profiles of SJP and MJP when the nozzle moves along a straight line. To keep the same material removal amount, the feed rate of SJP was set as 2.5 mm/min, whereas the feed rate of MJP was set as 20 mm/min. The dwell time on different positions was obtained by dividing the number of dwell positions by the total polishing time. Under the same material removal amount, it is interesting to note that the material removal width of MJP was larger than that of SJP, while the material removal depth was smaller. This smoother material removal profile was likely to allow MJP to achieve a lower MSF error [16,32]. On the other hand, when the nozzle moved along a straight line in MJP, some small peaks appeared at the bottom of the material removal cross-section profiles as shown in Fig. 2(b2) and Fig. 2(c2). When the path spacing was determined, the distribution of these small peaks affected the surface generation directly. In Fig. 2(b3), the small peaks overlapped with each other, which was detrimental to the restraint of ripple generation.

Optics EXPRESS

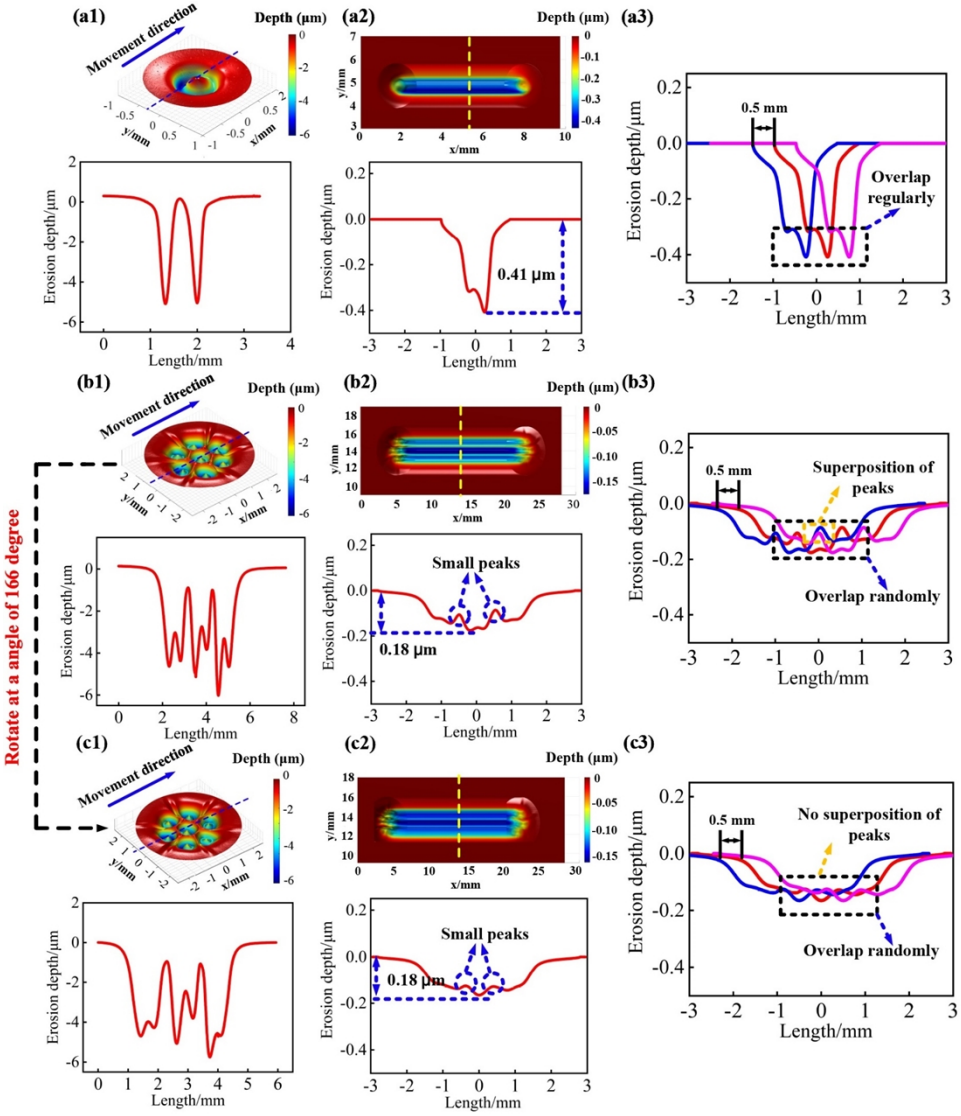

Fig. 2. Intuitive idea of suppressing MSF error by MJP. (a) SJP (b) MJP under nozzle orientation angle of 0 degrees, (c) MJP under nozzle orientation angle of 166 degrees. The numbers 1-3 refer to the three-dimensional TIF and corresponding cross-section profile in the x-direction, the material removal when the nozzle moves along a line path, and the corresponding cross-section profile in the y-direction, overlapping of material removal in different line paths, respectively.

Optics EXPRESS

However, after changing the nozzle orientation in Fig. 2(c2), the height of small peaks reduced as compared with Fig. 2(b2), and the superposition of these small peaks was well avoided in Fig. 2(c3). Based on the surface generation characteristics of MJP, it is essential to adjust the nozzle orientation in MJP to avoid the superposition of these small peaks and reduce the MSF error.

To investigate the feasibility of MJP in restraining MSF error, preliminary analysis and simulation comparison were conducted first. Figure 3 shows the simulation results of surface generation according to Eq. (1) and corresponding power spectral density (PSD) analyses after SJP and MJP under two different nozzle orientations. The tool path was a raster path and the path spacing was set as 0.5 mm. The material removal amount of MJP was kept the same as SJP by adjusting the feed rate. It was found that the height of the ripple was 0.32 μm after SJP, whereas the height of the ripple was reduced to 0.14 μm after MJP as shown in Fig. 3(a2) and Fig. 3(b2). The PSD spectrum in Fig. 3(a3) and Fig. 3(b3) also indicated that MJP can obtain a smaller MSF error in the position of spacial frequency 2 mm^{-1}. Hence, the simulation demonstrated that MJP had a better restraint ability for MSF error compared with SJP. After changing the nozzle orientation angle, the surface ripple height was restrained greatly from 0.14 μm to 0.014 μm as shown in Fig. 3(b2) and Fig. (c2). The PSD spectrum in Fig. 3(b3) and Fig. 3(c3) also indicated that the PSD magnitude of the generated surface was reduced well. The superposition of these small peaks in MJP led to an increase in ripple error. Adjusting the nozzle orientation angle can change the distribution of small peaks including the height and position. Hence, to achieve a lower MSF error, it is necessary to optimize the nozzle orientation angle and avoid the superposition of the small peaks under a specific path spacing.

In the following sections, MJP was utilized to validate the effectiveness and improve surface quality by restraining MSF error.

2.3. Experimental design

In MJP, the TIF is mainly determined by the arrangement of orifices in the nozzle. Hence, the distribution of orifices in the nozzle affects the MSF error directly. In this paper, a MJP tool with seven orifices was designed and fabricated. Figure 4 shows the distribution of orifices in the nozzle. The diameter of the orifice was 0.5 mm, while the distance between each orifice was 1 mm. To achieve a better polishing performance, the effect of nozzle orientation angle relative to the workpiece surface and path spacing on the MSF error was investigated. Three different nozzle orientation angles were selected to conduct the polishing experiment as shown in Fig. 4. Like other sub-aperture polishing processes, there is an edge removal effect in multi-jet polishing [33–36]. To avoid the edge effect, fixtures can be designed to extend the boundary of the workpiece surface and achieve a high form accuracy. On the other hand, SJP can be conducted to polish the workpiece edge after MJP so that the material removal distribution can be corrected [37]. In this paper, the edge effect is not discussed.

The polishing experiments were conducted on the MJP200 machine, which was purposely developed by the State Key Laboratory of Ultra-precision Machining Technology of Hong Kong Polytechnic University. The configuration of the machine is shown in Fig. 5. Five-axis (including X, Y, Z, A, and B axes) can realize linkage. The workpieces used in the experiments were NiCu alloy and HK9 optical glass. To avoid the effect of initial surface quality on the MSF error, the NiCu alloy and HK9 optical glass were machined by ultra-precision diamond turning and mechanical polishing first, respectively. The average surface roughness were 2.1 nm and 0.8 nm, respectively. The material removal of MJP and SJP was set at the same amount by adjusting the polishing feed rate under the same condition. To compare the performance of SJP and MJP considering the effect of path spacing and nozzle orientation angle, NiCu alloy was polished with 1000# SiC first. The polishing parameters were listed in Table 1.

Optics EXPRESS

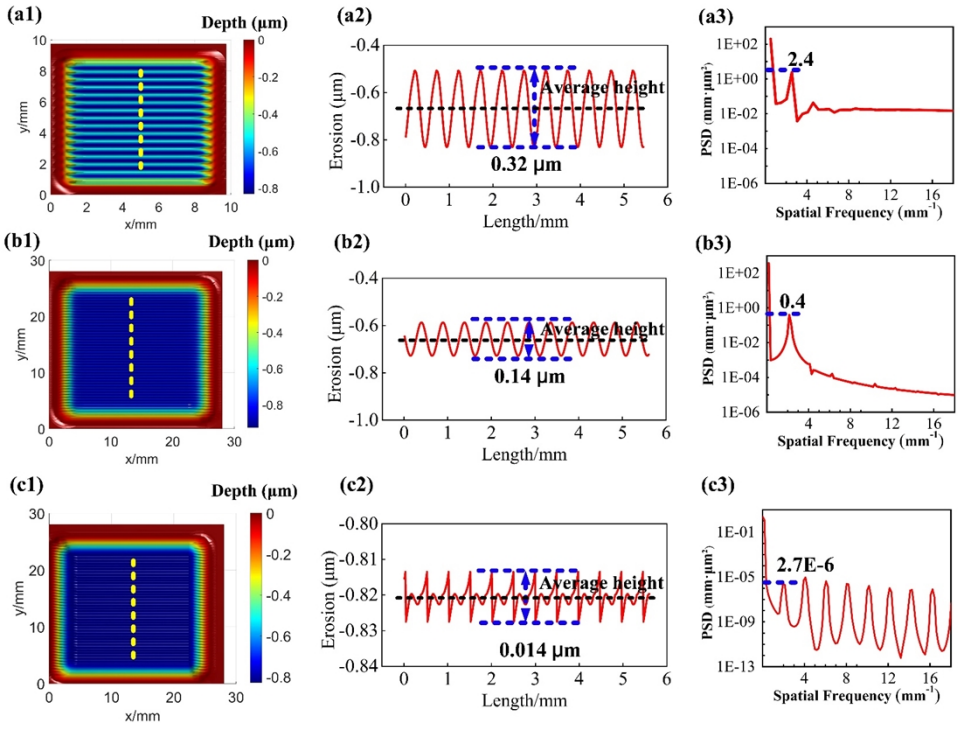

Fig. 3. The performance comparisons of MJP and SJP in reducing MSF error by simulations (a) SJP; (b) MJP under nozzle orientation angle of 0 degrees; (c) MJP under nozzle orientation angle of 166 degrees; The numbers 1-3 represent the simulated surface after polishing, cross-section profile of the generated surface, PSD spectrum of generated surface, respectively.

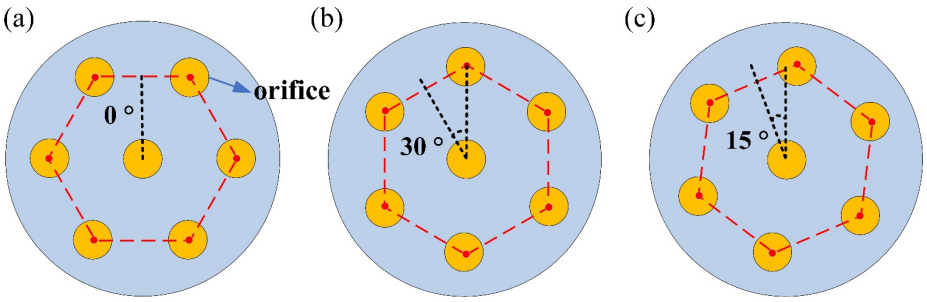

Fig. 4. The selected nozzle orientation angles and orifices distribution in MJP (a) MJP1 (b) MJP2 (c) MJP3.

Optics EXPRESS

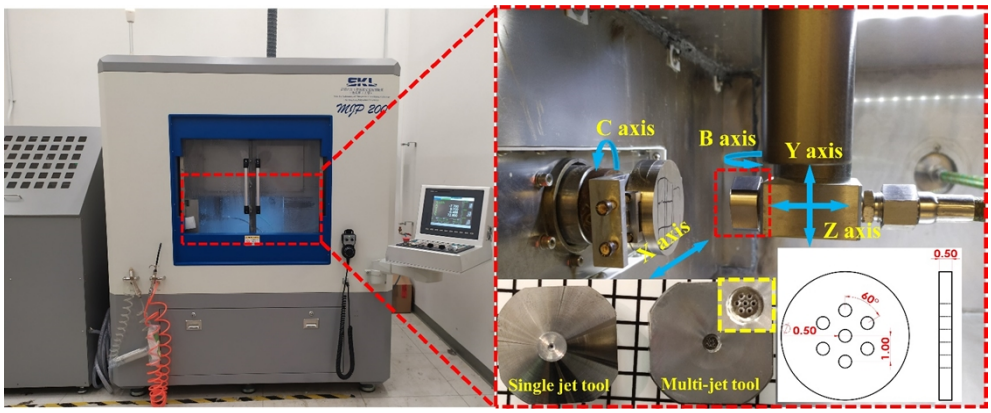

Fig. 5. The MJP machine utilized in experiments.

Table 1. Experiment parameters for the polishing of NiCu alloy

Parameters	Group 1	Group 2	Group 3	Group 4
Polishing tool	SJP	MJP1	MJP2	MJP3
Slurry	1000# SiC with a weight percentage of 8%			
Path spacing (mm)	0.1,0.2,0.3			
Feedrate (mm/min)	10	70		
Pressure (bar)	10			
Toolpath	Raster path			
Polishing area	10 mm*10 mm			
Stand-off distance (mm)	4 mm			

After validating the effectiveness of MJP, further optimization of nozzle orientation angle under different path spacings was conducted on NiCu alloy and HK9 glass. The abrasive utilized in the polishing of HK9 glass was Cerox 1663 cerium oxide with a weight percentage of 8% [38]. The diameter of cerium oxide abrasives is 1-2 µm.

2.4. Measurement methods

The surface morphologies and TIFs were measured by Zygo Nexview white light 3D interferometer. The surface roughness arithmetical mean height (*Sa*) and root mean square roughness value (*RMS*) after polishing were measured by atomic force microscope (AFM). The effective area was 10 µm × 10 µm to avoid the influence of ripples. The number of data points is 1024 × 1024, and the pixel resolution is about 10 nm. The value of arithmetic mean height *Sa* and root mean square roughness *RMS* were obtained by AFM software XEI directly. The PSD analysis was performed on the software MX.

3. Results and discussions

3.1. Performance of MJP in reducing MSF error

To avoid the change of slurry concentration when polishing for a long time, TIFs were measured before each group experiment as shown in Fig. 6. The TIFs were extracted by keeping the nozzle fixed relative to the NiCu alloy workpiece. The dwell time was 2 minutes. It can be seen that the TIF of SJP was closed to a 'W' shape. The flow field interference between adjacent jets, existing

Optics EXPRESS

in MJP, had a considerable impact on the erosion shape, which can be reflected in the line shape erosion between jets.

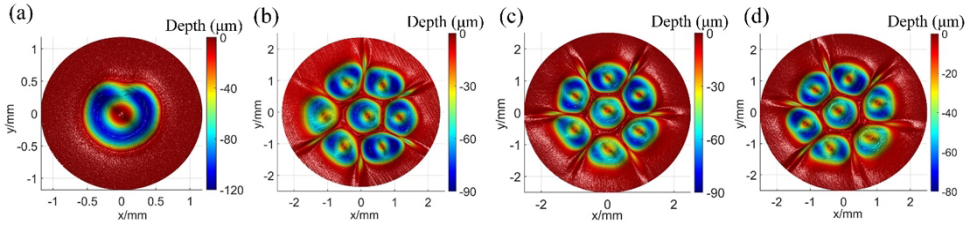

Fig. 6. Measured TIFs using different nozzles and nozzle orientation angles (a) SJP (b) MJP1 (c) MJP2 (d) MJP3.

Figure 7 shows the polishing results using SJP and MJP1 under different path spacings. When the path spacing was small (e.g., 0.1 mm and 0.2 mm), the material removal by SJP was not uniform, which was not found in MJP. When achieving the same material removal amount under the same polishing conditions, SJP should run at a lower feed rate. Hence, the nonuniform material removal for SJP may be caused by the fluctuation of polishing slurry concentration or the pump pressure for a long dwell time [39,40]. Furthermore, compared with SJP, MJP can achieve a smoother surface without ripple error. This also can be reflected by the PSD analysis in Fig. 8. After polishing with MJP, the PSD of the surface was reduced significantly under different path spacings. For example, when the path spacing was 0.3 mm, a high PSD peak appeared at the position of 3.3 mm^{-1} when polishing with SJP. However, after polishing with MJP1, the peak value of the PSD was reduced from 1 to 0.001. The polishing results demonstrated that MJP can restrain MSF error and achieve a higher surface quality.

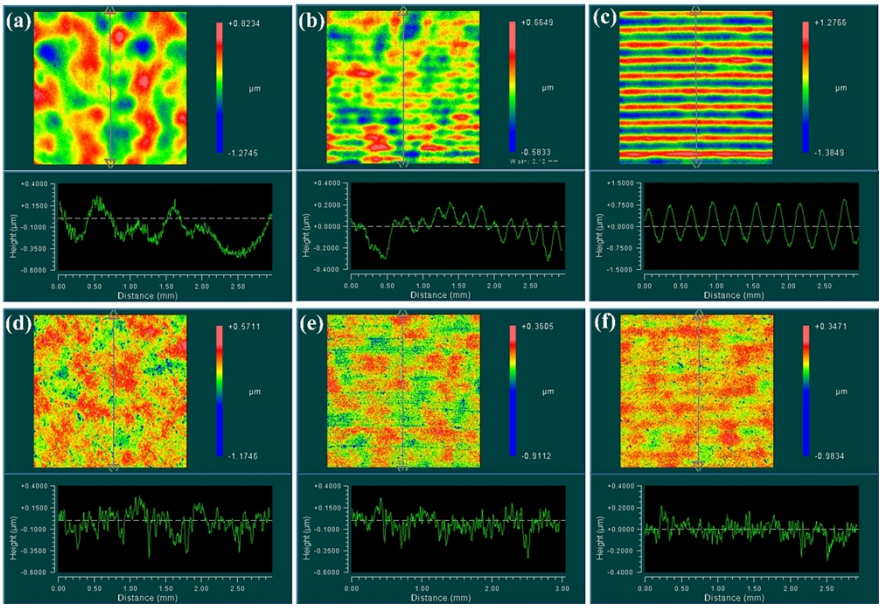

Fig. 7. The surfaces after polishing using SJP under different path spacings (a) 0.1 mm; (b) 0.2 mm; (c) 0.3 mm; and MJP1 under different path spacings (d) 0.1 mm; (e) 0.2 mm; (f) 0.3 mm.

Optics EXPRESS

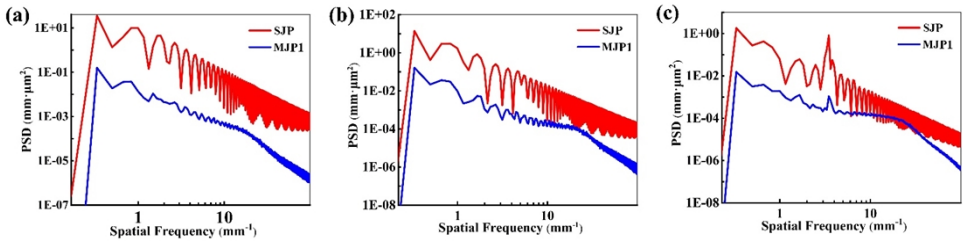

Fig. 8. PSD analysis of surfaces after SJP and MJP1 under different path spacings (a) 0.1 mm; (b) 0.2 mm; (c) 0.3 mm.

3.2. Effect analysis of nozzle orientation angle on MSF error in MJP

In FJP, when the polishing parameters and tool path are determined, the generated surface mainly depends on the material removal cross-section profile when the nozzle moves along a straight line relative to the workpiece. For MJP, when the nozzle orientation angle changes, the cross-section profile changes as well, which is different from the SJP. Therefore, it is the potential to achieve a lower MSF error by adjusting the nozzle orientation angle of MJP. Figure 9 shows the polishing results under different nozzle orientation angles and path spacings. When the path spacing was 0.1 mm, all three nozzle orientation angles including MJP1 in Fig. 7, MJP2, and MJP3 in Fig. 9 achieved a smooth surface without obvious ripple error. However, with the increase in path spacing, a noteworthy ripple appeared when using MJP2, whereas MJP1 and MJP3 still kept a high surface quality. When the path spacing was 0.3 mm, ripples were found for all three nozzle orientation angles. Figure 10 shows the surface PSD analyses under three different nozzle orientation angles. For MJP2, when the path spacing was larger than 0.1 mm, sharp peaks at the position of 5 mm^{-1} and 3.3 mm^{-1} appeared corresponding to the regular path spacings. Nonetheless, it is interesting to note that no peak was found when polishing using MJP1 and MJP3 even though the path spacing was 0.2 mm. When the path spacing increased to 0.3 mm, the PSD spectra of polished surfaces under all three nozzle orientation angles had some peaks. However, the peak value of MJP2 was far larger than that of the other two MJPs. It indicated that the nozzle orientation angle in MJP had a significant impact on the surface MSF error after polishing. An appropriate nozzle orientation angle under different path spacings should be optimized to restrain the MSF error effectively and achieve a high surface quality.

3.3. Optimization of nozzle orientation angle

To achieve a high surface quality with the lowest MSF error, it is necessary to optimize the nozzle orientation angle under different path spacings before polishing. In this section, the nozzle orientation angle was optimized based on the surface generation in FJP and then the optimization was validated by experiments.

In this optimization, the TIF of MJP1 $z = f(x,\ y)$ was utilized as the original data and the nozzle orientation angle was set as zero. When the nozzle orientation changed, the corresponding *TIF* $z' = f(x',\ y')$ can be obtained by translating and rotating the TIF, which was expressed as

$$\begin{bmatrix} x' \\ y' \\ z' \\ 1 \end{bmatrix} = \begin{bmatrix} 1 & 0 & 0 & -t_x \\ 0 & 1 & 0 & -t_y \\ 0 & 0 & 1 & 0 \\ 0 & 0 & 0 & 1 \end{bmatrix} \begin{bmatrix} cos\theta & -sin\theta & 0 & 0 \\ sin\theta & cos\theta & 0 & 0 \\ 0 & 0 & 1 & 0 \\ 0 & 0 & 0 & 1 \end{bmatrix} \begin{bmatrix} x \\ y \\ z \\ 1 \end{bmatrix} \tag{2}$$

Optics EXPRESS

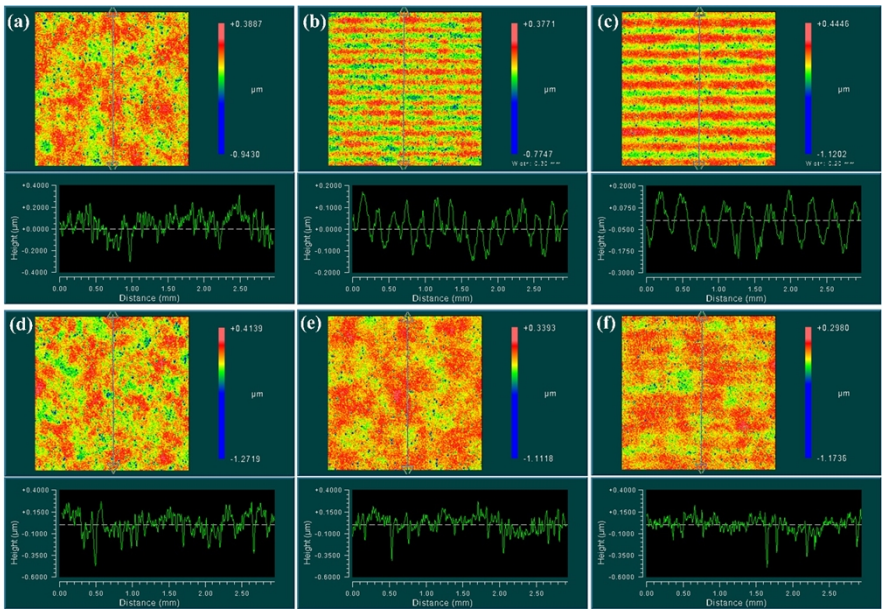

Fig. 9. The surfaces after polishing using MJP2 under different path spacings (a) 0.1 mm; (b) 0.2 mm; (c) 0.3 mm; and MJP3 under different path spacings (d) 0.1 mm; (e) 0.2 mm; (f) 0.3 mm.

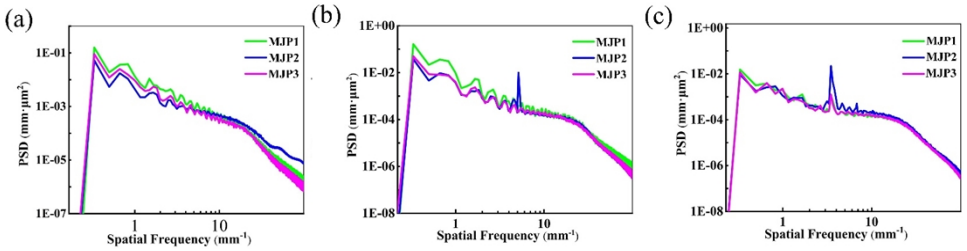

Fig. 10. PSD comparisons using MJP1, MJP2, and MJP3 under different pathing spacings (a) 0.1 mm; (b) 0.2 mm; (c) 0.3 mm.

Optics EXPRESS

where (t_x, t_y) was the coordinate of the *TIF* center measured by the Zygo interferometer; θ was the nozzle orientation angle and the unit is degree.

Figure 11 shows the nozzle orientation angle optimization process to reduce the MSF error. To evaluate the MSF error, different metrics were introduced such as root mean square roughness (RMS) [41], power spectral density (PSD) [42], and minimum modulation curve (MMC) [43]. In this study, the metric was the peak-to-value height (*PV*) of the cross-section profile of the polished surface [22,44]. To consider all the situations of the generated surface after polishing, the TIF was rotated from 0 to 180 degrees, respectively. The rotation angle interval was one degree. The *PV* values were calculated by the generated surfaces after every rotation. Finally, the smallest *PV* values and corresponding optimized orientation angles under different path spacings were obtained.

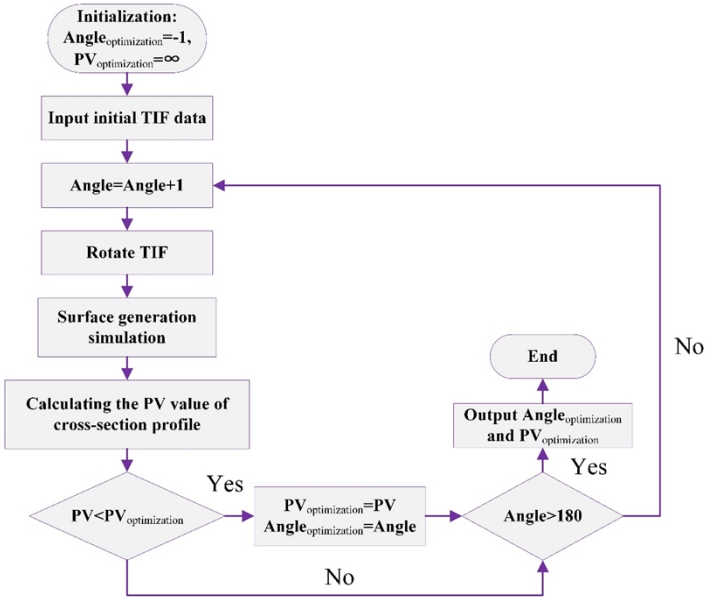

Fig. 11. Nozzle orientation angle optimization process.

To validate the optimization results, polishing experiments under different intervals were conducted using the optimized orientation angles. The optimized orientation angles were listed in Table 2.

Table 2. Optimized nozzle orientation angles under different intervals for NiCu alloy

Intervals (mm)	0.3 mm	0.5 mm	1.0 mm
Orientation angles (°)	29	156	21

Figure 12 shows the surface morphologies after polishing using the optimized nozzle orientation angles under different path spacings. Compared with the above polishing results, the height of the regular ripple was restrained well. The *PV* value of the cross-section profile was reduced from 0.12 μm to 0.07 μm under 0.3 mm of path spacing. Meanwhile, even though the path spacing increased to 0.5 mm and 1.0 mm, the height of the ripple still can be maintained at a low level below 0.16 μm. However, before optimizing the orientation angles in the polishing process, the ripple heights were 2.05 μm and 1.45 μm, respectively. Figure 13 shows the PSD analysis. The PSD magnitudes were reduced significantly under 0.5 mm and 1.0 mm path spacings. The

Optics EXPRESS

polishing results demonstrated that the optimization of nozzle orientation angles during MJP can further reduce the MSF error greatly.

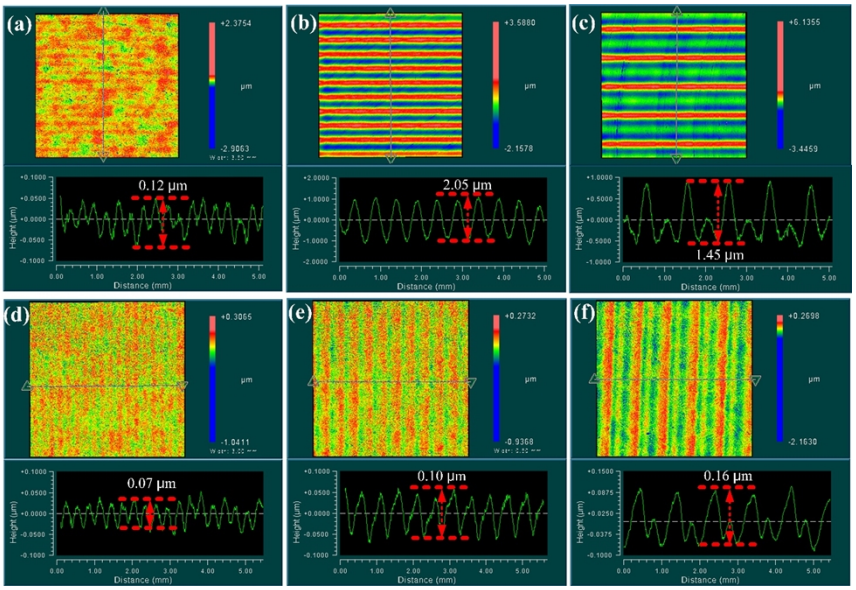

Fig. 12. The surfaces morphologies after polishing using MJP1 under path spacings (a) 0.3 mm, (b) 0.5 mm, (c) 1.0 mm, and optimized nozzle orientation angles under path spacings (d) 0.3 mm, (e) 0.5 mm, (e) 1.0 mm.

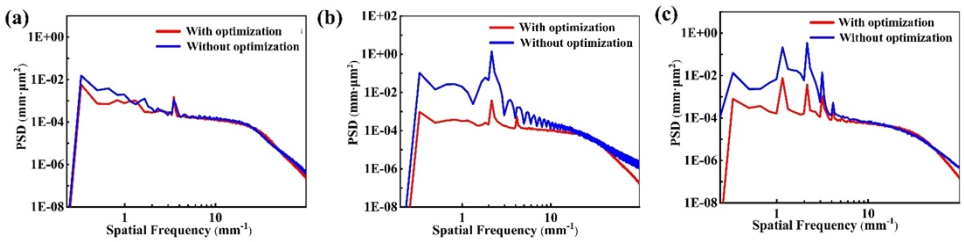

Fig. 13. PSD comparisons using the nozzle orientation angles with and without optimization under different path spacings, which are (a) 0.3 mm, (b) 0.5 mm, and (c) 1.0 mm path spacing, respectively. The TIF without optimization is corresponding to MJP1.

3.4. Polishing of HK9 optical glass

The above experimental results and theoretical analyses demonstrated MJP had a good maintenance ability to restrain the MSF error in FJP. The optimization agreed well with the experimental results, which can be utilized to improve the surface quality by adjusting the nozzle orientation angle under different path spacings. In the following section, to investigate the performance of MJP in the finishing of optical components, HK9 optical glass was utilized to conduct the polishing experiments and compare the polishing performance of traditional SJP and MJP. The polishing slurry was a mixture of cerium oxide abrasives and water with a weight ratio of 8:100. The initial TIF was extracted before polishing. The dwell time was 4 min. The measured TIFs are shown in Fig. 14. The nozzle orientation angles under different path spacings were optimized

Optics EXPRESS

according to section 3.3. The polishing parameters and optimized nozzle orientation angles under different path spacings are shown in Table 3 and Table 4, respectively.

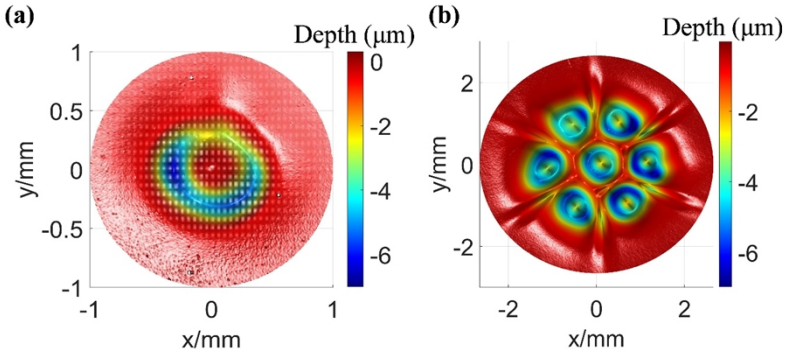

Fig. 14. The extracted TIFs of (a) SJP and (b) MJP in HK9 glass polishing.

Table 3. Polishing parameters of optical glass HK9

Polishing	Pressure (bar)	Feedrate (mm/min)	Stand-off distance (mm)	Path spacings (mm)
SJP	8	2.5	4	0.3, 0.5, 1.0
MJP	8	20	4	0.3, 0.5, 1.0

Table 4. Optimized nozzle orientation angles under different path spacings for optical glass HK9

Intervals/mm	0.3 mm	0.5 mm	1.0 mm
Orientation angles/°	11	166	159

Figure 15 shows the surface morphologies of HK9 glass after SJP and MJP. It is worth noting that MJP can improve the ripple error greatly under the same material amount. For MJP under the optimized nozzle orientation angles, there was no obvious ripple when the path spacings were 0.3 mm and 0.5 mm. The maximum *PV* of the cross-section profile was 17 nm when the path spacing was 1.0 mm. However, the ripple appeared on the surface after SJP even under a small path spacing of 0.3 mm. The *PV* values were 14 nm, 102 nm, and 133 nm, corresponding to the path spacings of 0.3 mm, 0.5 mm, and 1.0 mm, respectively. On the other hand, the PSD in Fig. 16 demonstrated that the peaks corresponding to the MSF error appeared in SJP with a high magnitude compared to MJP under the optimized nozzle orientation angles. For example, there was no PSD peak for MJP under 0.3 mm path spacing, whereas a significant peak at the position of 3.3 mm^{-1} appeared in SJP. When the path spacing increased, the number and magnitude of peaks in MJP were both smaller than that in SJP.

Figure 17 shows the surface morphologies measured by AFM after SJP and MJP. Under the same polishing conditions, the average surface roughness arithmetical mean height *Sa* and root mean square roughness *RMS* was 2.966 nm and 3.412 nm after MJP, which is similar to 2.932 nm and 3.425 nm achieved by SJP. Hence, MJP can achieve a low MSF error together with high efficiency without deteriorating the surface quality. It demonstrates that MJP has the same material removal process on the meta-microscale as compared with SJP.

On the other hand, the orifice distribution in the nozzle can affect the surface generation in MJP due to the change of TIF as described in section 2, which has an impact on the restraint of MSF error in MJP. Hence, the orifice distribution including the number and positions of orifices can be

Optics EXPRESS

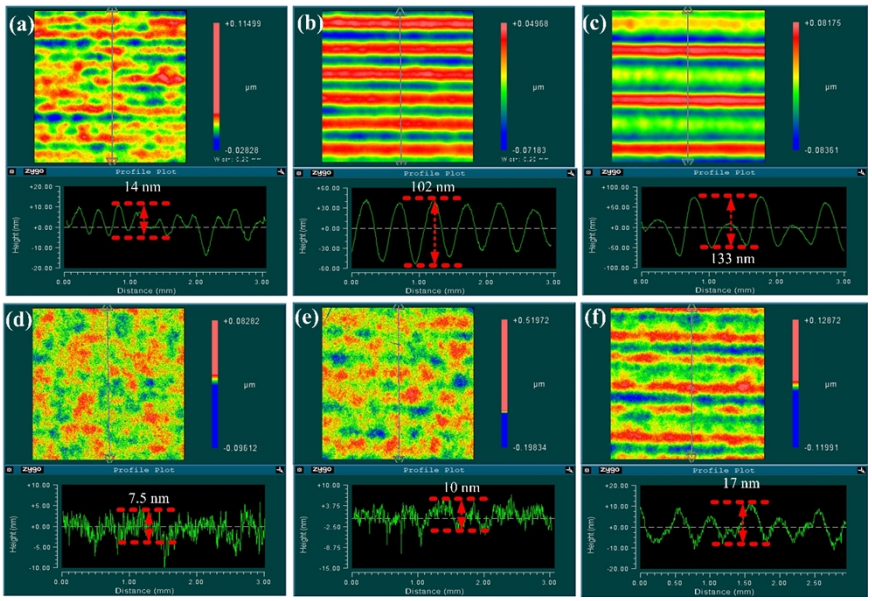

Fig. 15. The surfaces morphologies after SJP under path spacings (a) 0.3 mm, (b) 0.5 mm, (c) 1.0 mm, and MJP using the optimized nozzle orientation angles under path spacings (d) 0.3 mm, (e) 0.5 mm, (f) 1.0 mm.

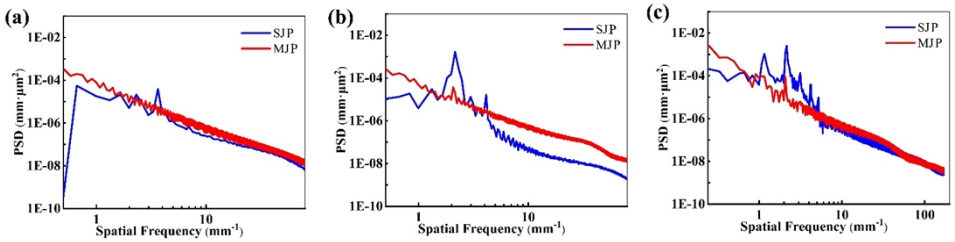

Fig. 16. PSD comparisons after MJP using the optimized orientation angles and SJP under path spacings (a) 0.3 mm, (b) 0.5 mm, (c) 1.0 mm.

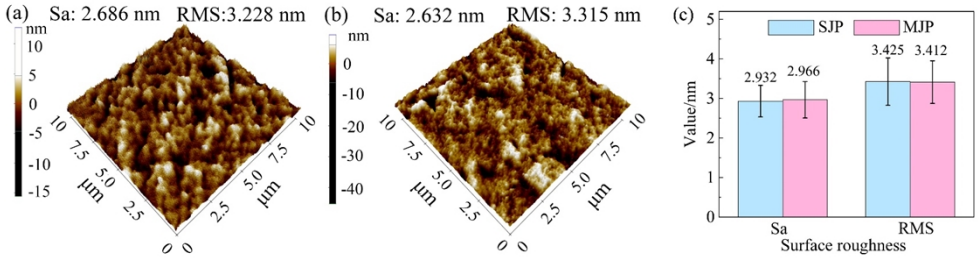

Fig. 17. surface morphologies measured by AFM after (a) SJP, (b) MJP, and (c) surface roughness Sa and RMS.

Optics EXPRESS

optimized. Figure 18 shows the potential orifice distributions such as array distribution, circular distribution, and triangular distribution. Combining with the theory developed in this paper, the nozzle orientation angles can be optimized under different orifice distributions, reducing the MSF error and achieving a better polishing performance. The corresponding work will be studied in detail in the future.

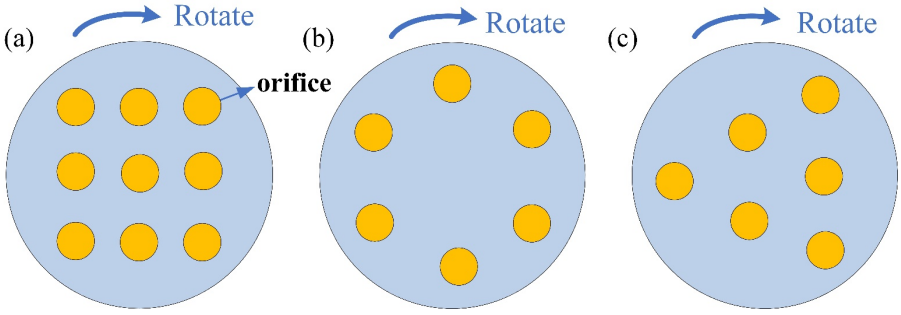

Fig. 18. Potential orifice distributions to achieve a lower MSF error (a) array distribution, (b) circular distribution, (c) triangular distribution

4. Conclusions

Restraining the MSF error remains challenging in computer controlled polishing technology. In this paper, a novel strategy was proposed to achieve a low MSF error by multi-jet polishing (MJP). Compared with traditional strategies, MJP can provide excellent operability, high effectiveness, and high efficiency. The key conclusions can be summarized as follows:

(1) Compared with traditional single jet polishing (SJP), the experimental results demonstrated that MJP can achieve a lower MSF error together with a higher polishing efficiency.

(2) The effect of different parameters on the MSF error, including polishing path spacing, and nozzle orientation angle, was investigated. Unlike SJP, the change of the nozzle orientation angle led to different MSF errors.

(3) An algorithm was built to optimize the nozzle orientation angle. According to the optimization of the nozzle orientation angle, low MSF error was obtained even under a large polishing path spacing in MJP. The effectiveness of MJP was validated by the polishing on NiCu alloy and optical HK9 glass.

(4) The difference between the polishing performance of SJP and MJP was revealed. Smoother material removal and refraining from the superposition of the small material removal peaks in MJP contributed to the reduction of MSF error.

The present work provides a new perspective on the restraint of MSF error in deterministic manufacturing. MJP has great potential to be used in the final finishing of optical components to achieve high performance and mass production.

Funding. Research and Innovation Office of the Hong Kong Polytechnic University (BBXL, BD9B, RK3M); Natural Science Foundation of Guangdong Province Program 2019–2020 (2019A1515012015); Research Grants Council of the Government of the Hong Kong Special Administrative Region, China (15200119).

Disclosures. The authors declare no conflicts of interest.

Data availability. Data underlying the results presented in this paper are not publicly available at this time but may be obtained from the authors upon reasonable request.

Optics EXPRESS

References

1. R. A. Jones, "Optimization of computer controlled polishing," Appl. Opt. **16**(1), 218–224 (1977).
2. T. Wang, L. Huang, M. Vescovi, D. Kuhne, Y. Zhu, V. S. Negi, Z. Zhang, C. Wang, X. Ke, H. Choi, W. C. Pullen, D. Kim, Q. Kemao, K. Nakhoda, N. Bouet, and M. Idir, "Universal dwell time optimization for deterministic optics fabrication," Opt. Express **29**(23), 38737–38757 (2021).
3. C. Wang, W. Yang, Z. Wang, X. Yang, C. Hu, B. Zhong, Y. Guo, and Q. Xu, "Dwell-time algorithm for polishing large optics," Appl. Opt. **53**(21), 4752–4760 (2014).
4. L. Zhang, Q. Z. Zhao, and C. Fan, "Dwell time algorithm in deterministic polishing of a free-form surface based on the continuous tool influence function," Appl. Opt. **60**(9), 2704–2715 (2021).
5. C. F. Cheung, C. J. Wang, L. T. Ho, and J. B. Chen, "Curvature-adaptive multi-jet polishing of freeform surfaces," CIRP Ann. **67**(1), 357–360 (2018).
6. Y. Mizoue, B. Sencer, and A. Beaucamp, "Identification and optimization of CNC dynamics in time-dependent machining processes and its validation to fluid jet polishing," Int. J. Mach. Tools Manuf. **159**, 103648 (2020).
7. C. F. Cheung, C. J. Wang, Z. C. Cao, L. T. Ho, and M. Y. Liu, "Development of a multi-jet polishing process for inner surface finishing," Precis. Eng. **52**, 112–121 (2018).
8. C. Wang, C. F. Cheung, M. Liu, and W. B. Lee, "Fluid jet-array parallel machining of optical microstructure array surfaces," Opt. Express **25**(19), 22710–22725 (2017).
9. C. J. Wang, C. F. Cheung, L. T. Ho, M. Y. Liu, and W. B. Lee, "A novel multi-jet polishing process and tool for high-efficiency polishing," Int. J. Mach. Tools Manuf. **115**, 60–73 (2017).
10. Y. J. Han, L. Zhang, C. Fan, W. L. Zhu, and A. Beaucamp, "Theoretical Study of Path Adaptability Based on Surface Form Error Distribution in Fluid Jet Polishing," Appl. Sci. **8**(10), 1814 (2018).
11. T. Wang, H. Cheng, H. Yang, W. Wu, and H. Tam, "Controlling mid-spatial frequency errors in magnetorheological jet polishing with a simple vertical model," Appl. Opt. **54**(21), 6433–6440 (2015).
12. J. M. Tamkin and T. D. Milster, "Effects of structured mid-spatial frequency surface errors on image performance," Appl. Opt. **49**(33), 6522–6536 (2010).
13. J. M. Tamkin, W. J. Dallas, and T. D. Milster, "Theory of point-spread function artifacts due to structured mid-spatial frequency surface errors," Appl. Opt. **49**(25), 4814–4824 (2010).
14. J. A. Shultz, M. A. Davies, and T. J. Suleski, "Effects of MSF errors on performance of freeform optics: Comparison of diamond turning and diamond milling," in *Imaging and Applied Optics 2015,* OSA Technical Digest (online) (Optical Society of America, 2015), FT4B.3.
15. R. N. Youngworth and B. D. Stone, "Simple estimates for the effects of mid-spatial-frequency surface errors on image quality," Appl. Opt. **39**(13), 2198–2209 (2000).
16. S. L. Wan, C. Y. Wei, Z. Hong, and J. D. Shao, "Modeling and analysis of the mid-spatial-frequency error characteristics and generation mechanism in sub-aperture optical polishing," Opt. Express **28**(6), 8959–8973 (2020).
17. C. R. Dunn and D. D. Walker, "Pseudo-random tool paths for CNC sub-aperture polishing and other applications," Opt. Express **16**(23), 18942–18949 (2008).
18. C. Wang, Z. Wang, and Q. Xu, "Unicursal random maze tool path for computer-controlled optical surfacing," Appl. Opt. **54**(34), 10128–10136 (2015).
19. Q. Zhao, L. Zhang, and C. Fan, "Six-directional pseudorandom consecutive unicursal polishing path for suppressing mid-spatial frequency error and realizing consecutive uniform coverage," Appl. Opt. **58**(31), 8529–8541 (2019).
20. A. Beaucamp, K. Takizawa, Y. J. Han, and W. L. Zhu, "Reduction of mid-spatial frequency errors on aspheric and freeform optics by circular-random path polishing," Opt. Express **29**(19), 29802–29812 (2021).
21. K. Takizawa and A. Beaucamp, "Comparison of tool feed influence in CNC polishing between a novel circular-random path and other pseudo-random paths," Opt. Express **25**(19), 22411–22424 (2017).
22. H. Y. Li, D. D. Walker, X. Zheng, X. Su, L. Z. Wu, C. Reynolds, G. Y. Yu, O. Li, and P. Zhang, "Mid-spatial frequency removal on aluminum free-form mirror," Opt. Express **27**(18), 24885–24899 (2019).
23. J. Zha, H. Zhang, Y. Li, and Y. Chen, "Pseudo-random Path Generation Algorithms and Strategies for the Surface Quality Improvement of Optical Aspherical Components," Materials **13**(5), 1216 (2020).
24. H. Hu, Y. Dai, and X. Peng, "Restraint of tool path ripple based on surface error distribution and process parameters in deterministic finishing," Opt. Express **18**(22), 22973 (2010).
25. J. Hou, D. Liao, and H. Wang, "Development of multi-pitch tool path in computer-controlled optical surfacing processes," J. Eur. Opt. Soc.-Rapid Publ. **13**(1), 22 (2017).
26. G. W. Wang, "Small Pitch Tool for Removing Middle Spatial Frequency Errors," in *Key Eng. Mater.* (Trans Tech Publ, 2013), 137–141.
27. J. Lin, C. Wang, H. Ye, W. Yang, and Y. Guo, "Effect of the tool influence function shape of the semirigid bonnet to the tool path ripple error," Opt. Eng **54**(11), 115104 (2015).
28. K. Wan, S. Wan, C. Jiang, C. Wei, and J. Shao, "Sparse bi-step raster path for suppressing the mid-spatial-frequency error by fluid jet polishing," Opt. Express **30**(5), 6603–6616 (2022).
29. C. Wang, H. Wang, R. Gao, J. Hou, S. Liu, M. Zhang, and X. Chen, "Investigation on the smoothing of surface spatial frequency errors for borosilicate glass by heat-treatment," J Manuf Process. **68**, 104–117 (2021).
30. W. Zhu and A. Beaucamp, "Zernike mapping of optimum dwell time in deterministic fabrication of freeform optics," Opt. Express **27**(20), 28692–28706 (2019).

Optics EXPRESS

31. Z. C. Cao, C. F. Cheung, and M. J. Ren, "Modelling and characterization of surface generation in Fluid Jet Polishing," Precis. Eng. **43**, 406–417 (2016).
32. T. Suratwala, J. Menapace, G. Tham, R. Steele, L. Wong, N. Ray, and B. Bauman, "Understanding and reducing mid-spatial frequency ripples during hemispherical sub-aperture tool glass polishing," Appl. Opt. **61**(11), 3084–3095 (2022).
33. W. Zhou, L. Zhang, C. Fan, T. Gu, and J. Zhao, "Investigation into material removal influenced by edge effect in polishing," Proc. Inst. Mech. Eng., Part B **231**(8), 1409–1422 (2017).
34. X. Ke, L. Qiu, C. Wang, and Z. Wang, "Tentative Investigations on Reducing the Edge Effects in Pre-Polishing the Optics," Appl. Sci. **10**(15), 5286 (2020).
35. B. Jiang, D. Zhao, B. Wang, H. Zhao, Y. Liu, and X. Lu, "Flatness maintenance and roughness reduction of silicon mirror in chemical mechanical polishing process," Sci. China: Technol. Sci. **63**(1), 166–172 (2020).
36. S. Wan, X. Zhang, W. Wang, M. Xu, and X. Jiang, "Edge control in precision robotic polishing based on space-variant deconvolution," Precis. Eng. **55**, 110–118 (2019).
37. P. Guo, H. Fang, and J. Yu, "Edge effect in fluid jet polishing," Appl. Opt. **45**(26), 6729–6735 (2006).
38. W. Q. Peng, C. L. Guan, and S. Y. Li, "Material removal mode affected by the particle size in fluid jet polishing," Appl. Opt. **52**(33), 7927–7933 (2013).
39. Y. Han, F. Duan, W. Zhu, L. Zhang, and A. Beaucamp, "Analytical and stochastic modeling of surface topography in time-dependent sub-aperture processing," Int. J. Mech. Sci. **175**, 105575 (2020).
40. Z. Guo, T. Jin, G. Xie, A. Lu, and M. Qu, "Approaches enhancing the process accuracy of fluid jet polishing for making ultra-precision optical components," Precis. Eng. **56**, 20–37 (2019).
41. D. M. Aikens, J. E. DeGroote, and R. N. Youngworth, "Specification and Control of Mid-Spatial Frequency Wavefront Errors in Optical Systems," in *Frontiers in Optics 2008/Laser Science XXIV/Plasmonics and Metamaterials/Optical Fabrication and Testing*, OSA Technical Digest (CD) (Optica Publishing Group, 2008), OTuA1.
42. A. Duparré, J. Ferre-Borrull, S. Gliech, G. Notni, J. Steinert, and J. M. Bennett, "Surface characterization techniques for determining the root-mean-square roughness and power spectral densities of optical components," Appl. Opt. **41**(1), 154 (2002).
43. H. Aryan, G. D. Boreman, and T. J. Suleski, "Simple methods for estimating the performance and specification of optical components with anisotropic mid-spatial frequency surface errors," Opt. Express **27**(22), 32709–32721 (2019).
44. C. Wang, W. Yang, S. Ye, Z. Wang, P. Yang, Y. Peng, Y. Guo, and Q. Xu, "Restraint of tool path ripple based on the optimization of tool step size for sub-aperture deterministic polishing," J. Adv. Manuf. Technol. **75**(9-12), 1431–1438 (2014).